Tribology International 38 (2005) 625–632

Characterization of lateral tape motion and disturbances in the servo position error signal of a linear tape drive

Jan Jose, Ryan J. Taylor*, Raymond A. de Callafon, Frank E. Talke

Center for Magnetic Recording Research, University of California at San Diego, 9500 Gilman Drive, La Jolla, CA 92093-0401, USA

Abstract

Lateral tape displacement in a tape drive is believed to be one of the critical limiting factors in achieving high track density in tape storage media. For improving track density, servo control systems can be designed on the basis of information from a position error signal to improve the track following capabilities in a tape drive. In this paper, we consider the characterization of lateral tape motion and additional disturbances that contribute to the position error signal. From a commercially available tape drive, the position error signal is measured electronically and lateral tape motion of the magnetic tape is measured using an optical edge sensor. This information is used to characterize the filtering effects of the disturbance rejection transfer function that determines the lateral tape motion and disturbances present in the position error signal. The disturbance rejection transfer function is characterized by two different methods. In the first method, we model the disturbance rejection transfer function as a simple high pass filter. Using lateral motion measurements as an input to this system, the position error signal is simulated and compared with the measured position error signal. In the second method, system identification methods are used to estimate a detailed high order filter that models the essential components of the disturbance rejection transfer function. Using these models, the position error signal is simulated and predicted and the effects of additional disturbances such as the servo track variability can be separated from the effects of the lateral tape motion. It is shown that the position error signal exhibits contributions from lateral tape motion and additional disturbances that differ significantly at higher frequencies.

Keywords: Lateral tape motion; Linear tape drive; Track misregistration

1. Introduction

Lateral displacement of tape in a modern tape drive is one of the critical factors in limiting the maximum track density on the tape [1]. Given current servo standards, lateral displacement can be successfully followed up to the control bandwidth of approximately 1 kHz. The bandwidth limitation of 1 kHz implies that lateral motion with frequency contents above 1 kHz cannot be followed by the servo system. As a result, high frequency lateral tape motion is considered to be a limiting factor in the ability to construct high track density tape storage systems. To analyze the performance of a tape servo system, in general high pass filtering of the lateral tape displacement is used to characterize the limiting amplitudes of motion, which cannot be followed at high frequencies. This filtering gives rise to a standard maximum amplitude of deviation given by a 6-sigma value. For quality purposes of the tape drive recording system, this maximum amplitude must be below 10% of the track width to avoid read and write errors (track misregistration).

Track misregistration (TMR) is the major consideration in pushing tape technology today to its areal density limits. The work by Arnett [2], Richards and Sharrock [1], and Dee [3] all report on the importance of increasing track density by using feedback servo control in disk and tape systems. Richards and Sharrock [1] point out that while linear bit density in tape has been steadily increasing over the past 50 years, track density has only recently started to increase with the same proportion. In the last 10 years, track density has increased from approximately 100 tracks per inch (TPI) to currently close to 1000 TPI. In the work by Dee [3] amplitude-based and timing-based servo systems in tape are compared, noting that timing-based systems de-emphasized cross-track amplitude linearity in the MR reader in

* Corresponding author.
E-mail address: taylor@talkevax.ucsd.edu (R.J. Taylor).

exchange for servo pattern writing accuracy. This means that the position error signal in timing-based servo is likely more affected by the accuracy of the servo pattern than in amplitude-based servo. The advantage to timing-based servo is that the position error signal is independent of head spacing modulation and tape speed [4].

In order to understand the effects of lateral tape displacement or lateral tape motion (LTM) on the TMR, we need to characterize the spectral contents and dynamics of disturbances acting on the servo system. With a better understanding of the spectral contents of the LTM and additional disturbances on the position error signal (PES), the design of the servo system can be tuned towards disturbance rejection for high track density recording. For that purpose, a standard high pass filtering of the LTM might not suffice to compute a standard maximum amplitude of deviation given by a 6-sigma value. More detailed information on the filtering effects of the disturbance rejection transfer function that determines the lateral tape motion and disturbances present in the position error signal is required. System identification has been used to identify dynamics of hard disk track following systems [5–7]. The method allows one to build a mathematical model of a dynamic system based on measured data. Aside from using this mathematical model to design feedback controllers, it can also be used to estimate the relative contribution of the different system disturbances to the position error signal. In tape systems, lateral tape motion, tape edge non-straightness, and servo track variability can all contribute to the position error signal.

In this paper, the filtering effects of the disturbance rejection transfer function is characterized by two different methods. In the first method, we model the disturbance rejection transfer function as a simple high pass filter. Using lateral motion measurements as an input to this system, the position error signal is simulated and compared with the measured position error signal. In the second method, system identification methods are used to estimate a detailed high order filter that models the essential components of the disturbance rejection transfer function. With the use of the estimated models, the position error signal is simulated and predicted more accurately and the effects of additional disturbances such as the servo track variability can be separated from the effects of the lateral tape motion. It is shown that the position error signal exhibits contributions from lateral tape motion and additional disturbances that differ significantly at higher frequencies.

2. The closed loop feedback control system and the sensitivity function

A commercial linear tape drive was used to perform the experiments in this study. The position error signal was measured from the drive electronics. Lateral tape displacement close to the head position was measured using an optical edge motion sensor [8]. This sensor gives a linear voltage when the light from transmitting fibers is partially blocked from receiving fibers.

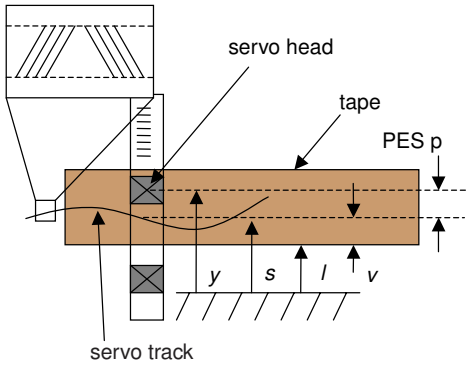

Fig. 1. Schematic of typical tape, servo head, and servo track with position error signal (PES) $p(t)$.

A schematic diagram of the tape, servo head, and servo track is shown in Fig. 1. The tape has servo tracks written on it so that the read head can be positioned on the data track. The position error signal is generated from the servo head using a timing-based servo pattern. For a time-based servo system, the time between consecutive events such as pulses or edges in the servo signal is related to the off track position of the head and is used to calculate the position error signal [4].

From Fig. 1, a number of variables used in this paper can be defined. The distance $y(t)$ is the servo head position with respect to a fixed reference, while $s(t)$ is the servo track position with respect to the same fixed reference. The distance $l(t)$ is the tape edge position with respect to the fixed reference, and $v(t)$ is the so-called servo track variability, defined as the difference between the servo track position $s(t)$ and the tape edge position $l(t)$. Finally, the position error signal $p(t)$ is defined as the difference between the servo head position $y(t)$ and the servo track position $s(t)$. Fig. 2 shows the block diagram for the closed loop feedback control system being investigated. This system consists of three inputs $l(t)$, $v(t)$, and $n(t)$, which represent the lateral tape displacement, the servo track variability, and measurement noise, respectively. The output of the system is the position error signal $p(t)$.

The system contains dynamics from the bulky read head (G) which is actuated by a voice coil motor (VCM). The VCM takes an input voltage $u(t)$ from the controller (C) and actuates the head position in an attempt to minimize the position error signal. The entire system can be thought of

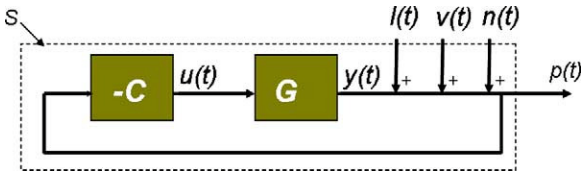

Fig. 2. Block diagram for the feedback control system.

as one box (the dashed line) or one sensitivity function denoted by S that translates the input to the output. To analyze this system, it is important to understand the relative contribution of each input to the output. For this analysis, the sensitivity function S is derived.

From Fig. 2, we have

$$u(t) = -Cp(t) \tag{2.1}$$

$$p(t) = Gu(t) - v(t) - l(t) - n(t) \tag{2.2}$$

where G and C denote convolution operators. Substitution of (2.2) into (2.1) yields

$$p(t) = \frac{1}{1+GC}v(t) + \frac{1}{1+GC}l(t) + \frac{1}{1+GC}n(t) \tag{2.3}$$

where

$$S = \frac{1}{1+GC} \tag{2.4}$$

is defined as the sensitivity function. For the analysis of the PES $p(t)$ we make a distinction between measurable and non-measurable signals. Since the lateral tape displacement $l(t)$ will be measured with an optical edge sensor, we consider $l(t)$ to be deterministic. Servo track variability $v(t)$ and (possible) electronic noise $n(t)$ cannot be measured and we model their effects as stochastic. The stochastic nature of $v(t)$ and $n(t)$ is characterized by a filtered white noise representation. The representations are given by

$$v(t) = H_v e_1(t) \tag{2.5}$$

$$n(t) = H_n e_2(t) \tag{2.6}$$

where $e_1(t)$ and $e_2(t)$ indicate white noise signals and H_v, H_n indicate a filtering with a stable and stably invertible noise filter, such that the spectrum Φ_v of $v(t)$ satisfies $\Phi_v = |H_v|^2$ and the spectrum Φ_n of $n(t)$ satisfies $\Phi_n = |H_n|^2$. Combining (2.3)–(2.6) gives

$$p(t) = Sl(t) + SH_v e_1(t) + SH_n e_2(t) \tag{2.7}$$

Since the servo track variability $v(t)$ and the electronic noise $n(t)$ are non-distinguishable, the stochastic signals are lumped together to compare their contribution to the position error signal directly to the contribution from the lateral tape position $l(t)$. Mathematically, we define

$$He(t) = S(H_v e_1(t) + H_n e_2(t)) \tag{2.8}$$

so that

$$p(t) = Sl(t) + He(t) \tag{2.9}$$

If we can estimate the sensitivity function S and the lateral tape displacement $l(t)$ is known as a function of time, then it can easily be determined what the relative contribution of each system driving signal is to the total position error signal. The characterization and estimation of the filtering effects of the sensitivity function S is discussed in Section 3.

3. Non-parametric estimation of the sensitivity function

3.1. Spectral estimate of S

To obtain a spectral estimate of the sensitivity function S, an estimate of the cross-spectral density between lateral tape displacement and position error signal is calculated. Estimates of the auto-spectral densities for each signal are also calculated and are shown in Fig. 3(a). The spectral estimate of the sensitivity function S is the ratio of the cross-spectral density to the auto-spectral density of the input. To calculate the cross-spectral density, each signal of N data points is broken up into K parts, where each part is N/K data points long. The Fourier transform is applied to each signal

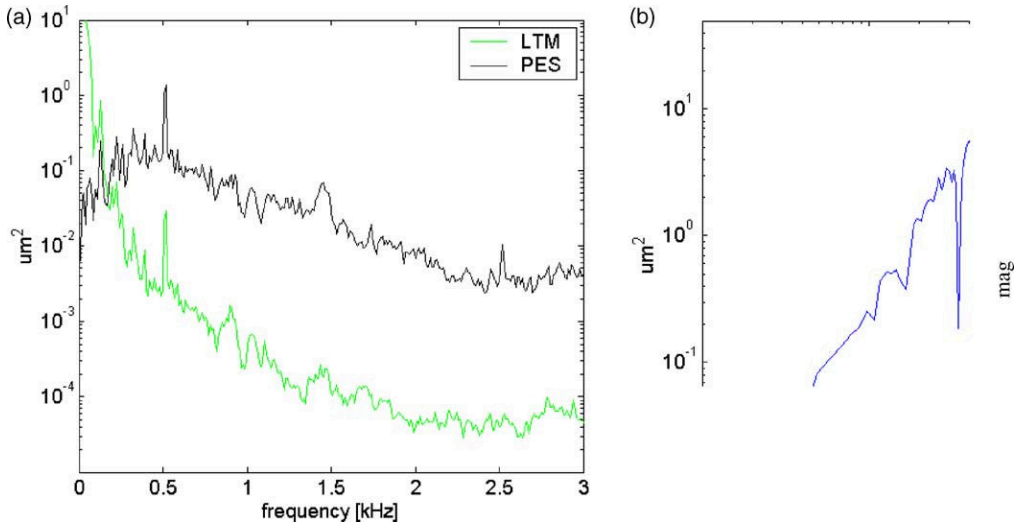

Fig. 3. (a) Power spectral densities of measured LTM and PES signals. (b) Spectral estimate of the sensitivity function S obtained from (3.5).

as follows

$$P_K(\omega) = \frac{N}{K} \sum_{t=1+(m-1)N/K}^{m(N/K)} p(t)\mathrm{e}^{-\mathrm{i}\omega t} \tag{3.1}$$

$$L_K(\omega) = \frac{N}{K} \sum_{t=1+(m-1)N/K}^{m(N/K)} l(t)\mathrm{e}^{-\mathrm{i}\omega t} \tag{3.2}$$

then the cross-spectral density is defined as

$$\hat{\Phi}_{lp}^K(\omega) = L_K^*(\omega)P_K(\omega) \tag{3.3}$$

while the auto-spectral density is defined as

$$\hat{\Phi}_{ll}^K(\omega) = L_K^*(\omega)L_K(\omega) \tag{3.4}$$

where the asterisk denotes the complex conjugation in each case.

Finally, the spectral estimate of the sensitivity function S is given as the ratio of the cross-spectral densities given in (3.3) and (3.4)

$$\hat{S}(\omega) = \frac{\hat{\Phi}_{lp}^K(\omega)}{\hat{\Phi}_{ll}^K(\omega)} \tag{3.5}$$

which is the quantity plotted in Fig. 3(b). Fig. 3(a) shows the estimates of the auto-spectral densities of typical lateral tape displacement and position error signals. We note that the lateral tape displacement signal contains more low frequency content than the PES. This is because the feedback control system is meant to follow the low frequency disturbances and fails to follow higher frequency disturbance. In this way, the system is similar to a high pass filter. The spectral estimate of the sensitivity function S shown in Fig. 3(b) is found to be similar to a high pass filter.

Since the sensitivity function is predominantly a high pass filter due to the limited bandwidth of the feedback control system, a simple high pass filter could be used to simulate the effect of lateral tape displacement on position error signal. A high pass filter (non-parametric estimation of S) is used in Section 3.2 to simulate the position error signal from the lateral tape displacement measurement.

3.2. Simulation of position error signal by high pass filtering

The most straightforward way to model the sensitivity function S is by assuming that it is a high pass filter. To simulate position error signal, lateral tape displacement signal was taken and used as the input to a 5th order Butterworth filter and compared to measured PES. The result is shown in Fig. 4(a) below. Only marginal agreement between 'simulated' PES (high pass filtered LTM) and measured PES is found. The filter used is shown with the sensitivity function S in Fig. 4(b). From this result, we observe that a more accurate representation of the sensitivity function S should be obtained. Parametric identification is used in Section 4 to simulate and predict position error signal more accurately.

4. Parametric identification of sensitivity function

To improve the prediction of the contribution of lateral tape motion to the position error signal of the servo system in a linear tape drive, a more detailed characterization of the sensitivity function S in (2.4) is required. A parametric estimation and optimization of a filter that models the sensitivity function S will provide not only a better model for the filtering effect of the lateral tape motion on the PES, it will also provide a characterization of the spectral contents of the servo track variability $v(t)$ and electronic noise $n(t)$ present on the position error signal. In this way we are able to characterize and compare the relative

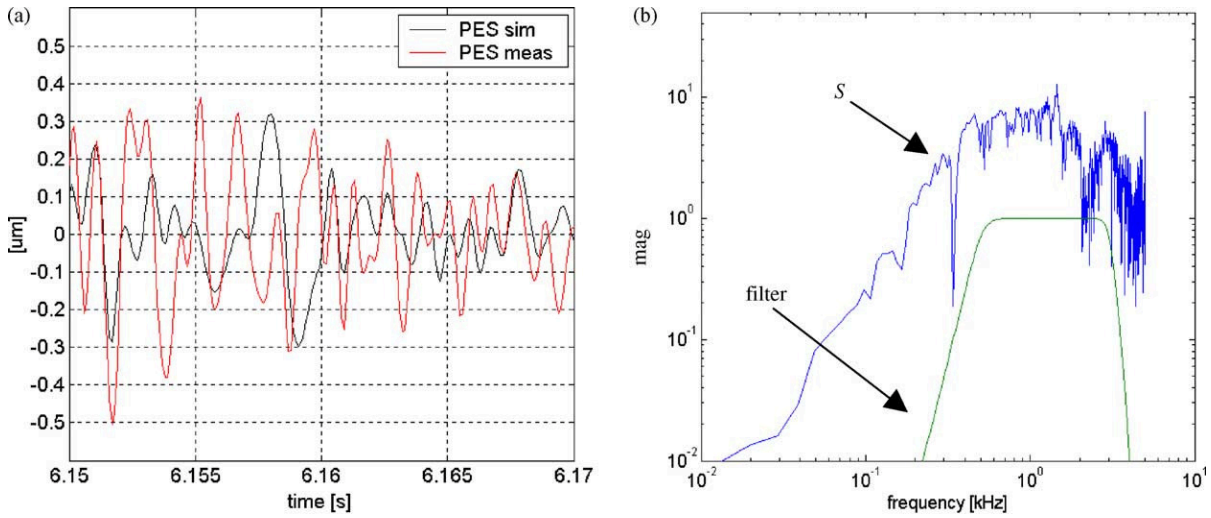

Fig. 4. (a) Comparison of simulated PES (high pass filtered LTM), and measured PES. (b) 5th order Butterworth filter used for simulation of PES.

contribution of the LTM $l(t)$ and the sum of the track variability and electronic noise $n(t)$ in the position error signal $p(t)$.

For the identification of a model $\hat{S}$ of the sensitivity function S and the characterization of the spectral contents H of the additional disturbances $v(t)$ and $n(t)$ on the position error signal, the standard prediction error framework [9] is adopted. To complete this paper, the prediction error framework is reviewed here but one is referred to [9] for a complete discussion.

4.1. Prediction error framework

For the identification of the model $\hat{S}$ of the sensitivity function S, we consider discrete time domain measurements of the LTM $l(t)$ and the position error signal (PES) $p(t)$ over $t=1,2,\ldots,N$ and assume a causal relationship between the input signal $l(t)$ and the output signal $p(t)$ to estimate a discrete time filter $\hat{S}(q)$ of the sensitivity function S. In the prediction error framework, the prediction of the output $p(t)$ on the basis of previous measurements $l(s)$, $s=1,\ldots,t-1$ is optimized over a free parameter θ. The one-step ahead prediction of the PES $p(t)$ on the basis of previous measurements is denoted by

$$p(t|t-1,\theta) = H(q,\theta)^{-1}S(q,\theta)l(t) - (H(q,\theta)^{-1}-1)p(t) \tag{4.1}$$

where $S(q,\theta)$ represents the parametrized discrete time filter of the sensitivity function S and $H(q,\theta)$ denotes the parametrized noise model that will model the spectral contents H of the additional disturbances $v(t)$ and $n(t)$ on the PES $p(t)$.

The parameter θ is used to denote the unknown parameters of the models $S(q,\theta)$ and $H(q,\theta)$ to be estimated. With the prediction $p(t|t-1)$ of the PES $p(t)$ given in (4.1), the prediction error is defined by

$$\varepsilon(t,\theta) := p(t) - p(t|t-1,\theta) = H(q,\theta)^{-1}[p(t) - S(q,\theta)l(t)] \tag{4.2}$$

and the parameter estimate $\hat{\theta}$ is determined by minimizing the 2-norm of the (filtered) prediction error $\varepsilon_f(t,\theta)$ and given by

$$\hat{\theta} := \arg\min_{\theta} \sum_{t=1}^{N} \varepsilon_f(t,\theta)^2, \quad \varepsilon_f(t,\theta) = F(q)\varepsilon(t,\theta) \tag{4.3}$$

where $F(q)$ denotes an additional discrete time filter that can be used to emphasize or de-emphasize a certain frequency region of the prediction of the PES $p(t)$.

In general, the computation of the optimal parameter estimate $\hat{\theta}$ in (4.3) requires a non-linear optimization. To facilitate the optimization in (4.3), a specific parameterization is chosen for the discrete time filter $S(q,\theta)$ of the sensitivity function S and the noise filter $H(q,\theta)$ that models the spectral contents of the $v(t)$ and $n(t)$. The filters $S(q,\theta)$ and $H(q,\theta)$ are parametrized in a standard linear regression or AutoRegressive with eXogenous input (ARX) model structure [9]

$$S(q,\theta) = B(q,\theta)/A(q,\theta), \quad H(q,\theta) = 1/A(q,\theta) \tag{4.4}$$

where $A(q,\theta)$ and $B(q,\theta)$ are polynomials of the discrete time filter in the format

$$\begin{aligned} B(q,\theta) &= b_0 + b_1 q^{-1} + b_2 q^{-2} + \cdots + b_n q^{-n}, \\ A(q,\theta) &= 1 + a_1 q^{-1} + a_2 q^{-2} + \cdots + a_n q^{-n} \end{aligned} \tag{4.5}$$

and the parameter vector θ is given by $\theta = \begin{bmatrix} b_0 & b_1 & \cdots & b_n & a_1 & a_2 & \cdots & a_n \end{bmatrix}$. The optimization in (4.3) using the linear regression model structure (4.4) and (4.5) boils down to a standard (weighted) least-squares solution that can be computed without an iterative minimization.

It should be noted that the ARX model structure parametrization in (4.4) is restrictive, as it assumes common poles between discrete time filter $S(q,\theta)$ and the noise filter $H(q,\theta)$, and it does not estimate zeros in the noise filter $H(q,\theta)$. However, if a large model order n in (4.5) is permitted, an ARX model can provide accurate estimates of filter and noise dynamics [10]. In this paper, the objective is to find an accurate simulation and prediction of the PES $p(t)$ due to the effects of the LTM $l(t)$ and the external noise sources $n(t)$ and $v(t)$ present on the PES $p(t)$. As a consequence, no particular restrictions on the order of the filters $S(q,\theta)$ and $H(q,\theta)$ is imposed and the ARX model parameterization can be used for estimation purposes.

4.2. Estimation results

The experimental setup discussed in Section 2 was used to measured input/output data sequence of the LTM $l(t)$ and the PES $p(t)$, $t=1,2,\ldots,N$ over $N=10^6$ data points. For the computation of the optimal parameter estimate $\hat{\theta}$ in (4.3) of the models $\hat{S}=S(q,\hat{\theta})$ and $\hat{H}=H(q,\hat{\theta})$ only the first $N=50{,}000$ data points were used. The remaining part of the data is only used to evaluate the simulation and prediction capabilities of the models being estimated.

To obtain accurate prediction and simulation capabilities with the ARX model structure in (4.4), a model order of $n=40$ is chosen for the polynomials $A(q,\theta)$ and $B(q,\theta)$ in (4.5). As indicated in Section 4.1, accurate results with an ARX model structure are obtained, provided that the model order n is not restricted [10]. Since the models $\hat{S}=S(q,\hat{\theta})$ and $\hat{H}=H(q,\hat{\theta})$ are only used for simulation and prediction purposes, no immediate restriction on the model order n is required. However, it was found that increasing the model order beyond $n=40$ did not significantly improve the simulation and prediction capabilities of the models $\hat{S}=S(q,\hat{\theta})$ and $\hat{H}=H(q,\hat{\theta})$. The separation of the experimental data in a part used for estimation purposes and a part for

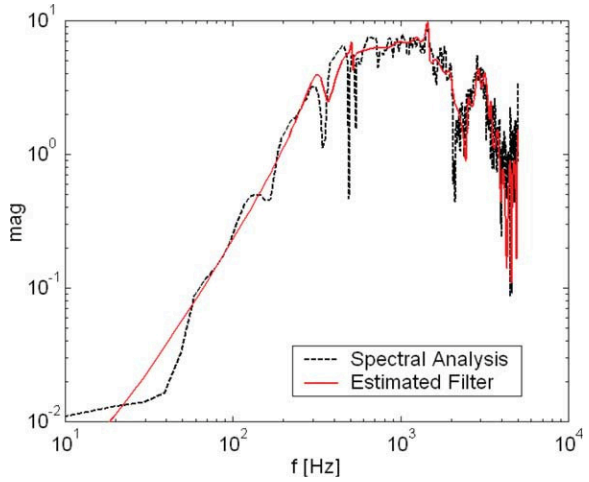

Fig. 5. Amplitude Bode plot of spectral estimate $\hat{S}(\omega)$ (dashed line) and 40th order parametric model $\hat{S} = S(q, \hat{\theta})$ (solid line).

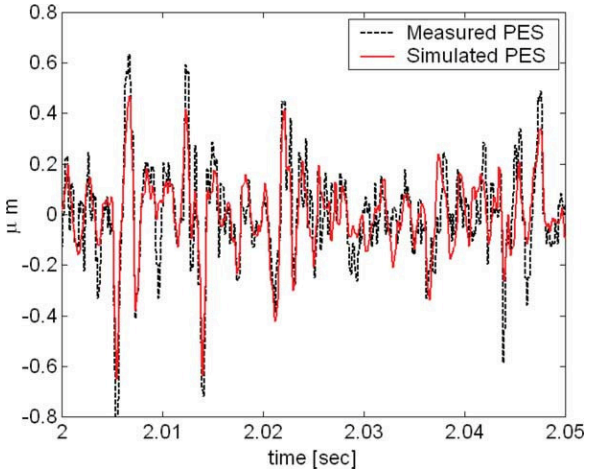

Fig. 6. Comparison of measured PES $p(t)$ (dashed line) and simulated PES $p_{\text{sim}}(t)$ given in (4.6) (solid line).

simulation and prediction purposes is necessary to avoid 'overfitting' of the data [9] by choosing using an unnecessarily high model order. As result, 40th order models $\hat{S} = S(q, \hat{\theta})$ and $\hat{H} = H(q, \hat{\theta})$ are obtained to simulate and predict the PES $p(t)$ due to the LTM $l(t)$ and the additional noise disturbances $v(t)$ and $n(t)$. The estimation result for the models is depicted in the following figures.

To illustrate the improvement on the details of the high pass filtering effects of the sensitivity function S, a comparison is made in Fig. 5 between the spectral estimate $\hat{S}(\omega)$ and the 40th order parametric (high pass) filter $\hat{S} = S(q, \hat{\theta})$ being estimated by the identification procedure. It can be seen from Fig. 5 that a more detailed filter is found that also models the high frequency resonance modes typically found in the sensitivity function of a servo controlled mechanical system.

The more detailed characterization of the filtering effects in the sensitivity function S that are captured in the model $\hat{S} = S(q, \hat{\theta})$ is also confirmed by the simulation of the PES

$$p_{\text{sim}}(t) = S(q, \hat{\theta}) l(t) \tag{4.6}$$

where $l(t)$ indicates the measured LTM signal that was not used for estimation purposes of the filter $\hat{S} = S(q, \hat{\theta})$. A comparison of the measured PES $p(t)$ and the simulated PES $p_{\text{sim}}(t)$ is depicted in Fig. 6, where it can be seen that a much better agreement is found than by standard high pass filtering. It can also be observed that there is still a discrepancy between the simulated and measured PES. This is due to the fact that $p_{\text{sim}}(t)$ in (4.6) only simulates the effect of the lateral tape motion $l(t)$. Obviously, variations in the PES $p(t)$ are not caused by lateral tape motion $l(t)$ only as indicated in the block diagram of Fig. 2.

To predict the (combined) effect of the servo track variability $v(t)$ and the (possible) electronic noise $n(t)$, the prediction of the PES $p(t)$ can be computed via

$$p_{\text{pred}}(t) = H(q, \hat{\theta})^{-1} S(q, \hat{\theta}) l(t) - (H(q, \hat{\theta})^{-1} - 1) p(t) \tag{4.7}$$

where $l(t)$ and $p(t)$ now indicate the measured LTM signal and PES that were not used for estimation purposes. The formulation of the prediction $p_{\text{pred}}(t)$ is based on (4.1) and uses previous values of $l(s)$ and $p(s)$, $s = 1,2,\ldots,t-1$ to predict the PES $p(t)$ at time t. Since this is done on data that has not been used during the estimation process of the models $\hat{S} = S(q, \hat{\theta})$ and $\hat{H} = H(q, \hat{\theta})$, we can evaluate the one-time-step ahead prediction capabilities of the models. The result is plotted in Fig. 7 over the same time span as used in Fig. 6. It can be observed that by using both the filter model $\hat{S} = S(q, \hat{\theta})$ to predict the effect of the LTM $l(t)$ and the noise model $\hat{H} = H(q, \hat{\theta})$ to predict the combined effect of $n(t)$ and $v(t)$, a much better prediction of the PES $p(t)$ is obtained.

5. Relative disturbance characterization on the PES

With the estimated models $\hat{S} = S(q, \hat{\theta})$ and $\hat{H} = H(q, \hat{\theta})$ a comparison can be made on the relative contribution of

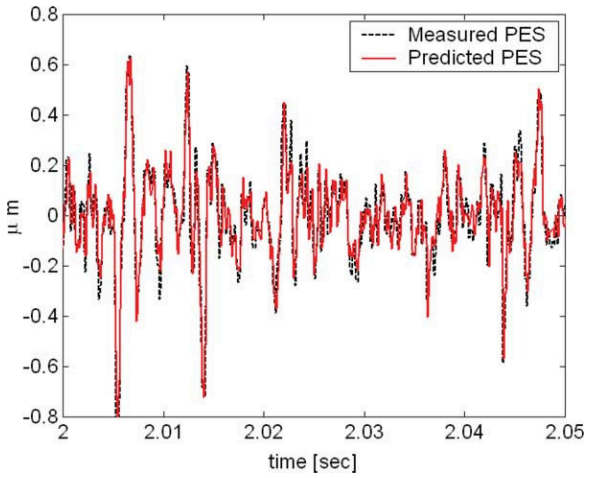

Fig. 7. Comparison of measured PES $p(t)$ (dashed line) and predicted PES $p_{\text{pred}}(t)$ given in (4.7) (solid line).

the LTM $l(t)$ and the combined disturbance effect $d(t)$ of the servo track variability $v(t)$ and the (possible) electronic noise $n(t)$. This gives insight in the distribution of the spectral contents of the different disturbances that act on the servo system of the tape drive. Since the PES $p(t)$ is modeled by

$$p(t) = S(q,\hat{\theta})l(t) + d(t), \quad d(t) = H(q,\hat{\theta})e(t) \tag{5.1}$$

where $e(t)$ is a white noise signal with variance λ, the relative contribution of the LTM $l(t)$ and the disturbances $d(t)$ can be separated. Under the viable assumption that the LTM $l(t)$ is uncorrelated with the additional disturbances $d(t)$ on the PES $p(t)$ (such as servo track variability $v(t)$ and electronic noise $n(t)$), the auto spectrum $\Phi_{pp}(\omega)$ of the PES $p(t)$ is given by

$$\Phi_{pp}(\omega) = |S(e^{jw},\hat{\theta})|^2\Phi_{ll}(\omega) + |H(e^{jw},\hat{\theta})|^2\lambda \tag{5.2}$$

Separation is now possible as the LTM signal $l(t)$ is measured and the effect of $l(t)$ on the PES $p(t)$ is modeled by $S(q,\hat{\theta})$. As a result, the relative contribution $|S(e^{jw},\hat{\theta})|^2\Phi_{ll}(\omega)$ of the LTM $l(t)$ and the contribution $|H(e^{jw},\hat{\theta})|^2\lambda$ of the additional noise $d(t)$ on the PES $p(t)$ can be estimated by

$$\begin{aligned}\hat{\Phi}^{l}_{pp}(\omega) &= |S(e^{jw},\hat{\theta})|^2\hat{\Phi}_{ll}(\omega),\\ \hat{\Phi}^{d}_{pp}(\omega) &= |H(e^{jw},\hat{\theta})|^2\hat{\lambda}\end{aligned} \tag{5.3}$$

where $\hat{\Phi}_{ll}(\omega)$ denotes the estimate of the auto spectrum of $l(t)$ and $\hat{\lambda}$ denotes the estimate of the variance of the prediction error in (4.2). $\hat{\Phi}^{l}_{pp}(\omega)$ denotes the modeled spectral contents of the PES $p(t)$ due to the LTM $l(t)$. Similarly, $\hat{\Phi}^{d}_{pp}(\omega)$ denotes the modeled spectral contents of the PES $p(t)$ due to additional disturbances $d(t)$ such as electronic noise and tape edge variation. Since all quantities in (5.3) are known when an estimation of the models $\hat{S} = S(q,\hat{\theta})$ and $\hat{H} = H(q,\hat{\theta})$ is available, the relative contribution of the LTM and other disturbances on the servo system of the tape drive can be plotted over a specific frequency range. The result has been depicted in Fig. 8, where a comparison is made with a standard spectral estimate [11] of the relative contribution of the input and disturbance spectrum

$$\begin{aligned}\hat{\Phi}^{l*}_{pp}(\omega) &= \left|\frac{\hat{\Phi}_{lp}(\omega)}{\hat{\Phi}_{ll}(\omega)}\right|^2\hat{\Phi}_{ll}(\omega) = \frac{|\hat{\Phi}_{lp}(\omega)|^2}{\hat{\Phi}_{ll}(\omega)},\\ \hat{\Phi}^{d*}_{pp}(\omega) &= \hat{\Phi}_{pp}(\omega) - \left|\frac{\hat{\Phi}_{lp}(\omega)}{\hat{\Phi}_{ll}(\omega)}\right|^2\hat{\Phi}_{ll}(\omega)\\ &= \hat{\Phi}_{pp}(\omega) - \frac{|\hat{\Phi}_{lp}(\omega)|^2}{\hat{\Phi}_{ll}(\omega)}\end{aligned} \tag{5.4}$$

It can be seen from Fig. 8 that the models $\hat{S} = S(q,\hat{\theta})$ and $\hat{H} = H(q,\hat{\theta})$ follow the general trend in the (noisy) spectral estimate of (5.4) very well, confirming the good quality of the models being estimated. More importantly, it

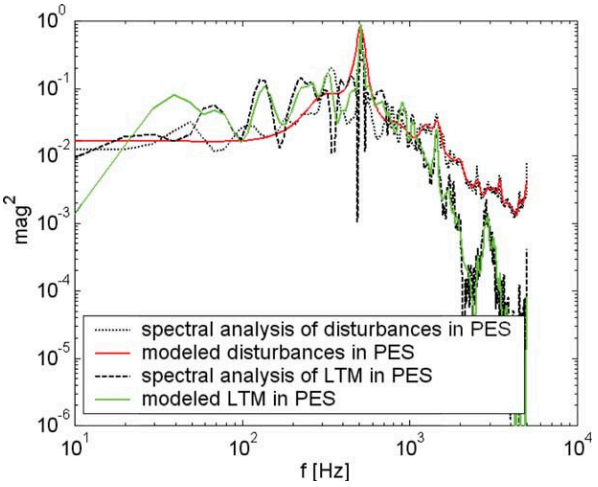

Fig. 8. Spectral content of LTM $\hat{\Phi}^{l*}_{pp}(\omega)$ (dashed) and disturbance $\hat{\Phi}^{d*}_{pp}(\omega)$ (dotted) of auto spectrum $\Phi_{pp}(\omega)$ of PES as defined in (5.4) and modeled contribution of LTM $\hat{\Phi}^{l}_{pp}(\omega)$ (2nd solid) and disturbances $\hat{\Phi}^{d}_{pp}(\omega)$ (1st solid) according to (5.3).

can be observed that the relative contribution of the additional disturbances $d(t)$, such as servo track variability $v(t)$ and electronic noise $n(t)$, have a larger contribution on the PES $p(t)$ than the LTM $l(t)$ at frequencies above approximately 1 kHz. At lower frequencies, the LTM has a slightly larger contribution. This is in conformance with the estimated spectrum of the LTM as depicted in Fig. 3(a). In light of the servo system for the tape drive with its limited bandwidth capacity, it is important to take into account the reduction and nature of the additional disturbances such as servo track variability $v(t)$, as it has a larger impact at higher frequencies.

6. Conclusions

Two methods were used to simulate and predict the effect of lateral tape motion on the position error signal of a servo system in a linear tape drive system. The methods are based on the optical measurement of lateral tape motion and availability of a position error signal (PES) measurement for estimation and validation purposes. In the first method, the lateral tape displacement signal was high pass filtered to estimate the filtering effects of the disturbance rejection transfer function. This result gives only a fair to poor agreement between the measured PES and simulated PES. In a second method, a prediction error-based system identification was used to estimate a parametric filter to model the dynamics of disturbance rejection transfer function and the spectral content of additional noise disturbances present on the PES. Using lateral tape displacement as an input to this model, PES was simulated and predicted and reasonable agreement to measured PES was achieved.

It was observed that lateral tape displacement has a significant low frequency content that is controlled by

the servo system. In addition, the lateral tape displacement has a high frequency contribution that affects the PES well above the 1 kHz bandwidth limitation of the servo system. Aside from the high frequency effects of the lateral tape displacement, additional disturbances on the PES were observed that have even a larger impact at high frequencies. These disturbances include servo track variability and possible electronic noise in measuring the PES for servo purposes.

References

[1] Richards DB, Sharrock MP. Key issues in the design of magnetic tapes for linear systems of high track density. IEEE Trans Magn 1998; 34(4).

[2] Arnett P, Tsang C, Diola T, Vo L. TMR considerations at 5 Gb/in.^{2} and 10 Mb/s. IEEE Trans Magn 1997;33(5).

[3] Dee R. Magnetic tape recording technology and devices. International non-volatile memory technology conference 1998.

[4] Barrett RC, Klaassen EH, Albrecht TR, Jaquette GA, Eaton JH. Timing-based track-following servo for linear tape systems. IEEE Trans Magn 1998;34(4):1872–7.

[5] Van den Hof PMJ, de Callafon RA, van Donkelaar E. CLOSID—a Matlab toolbox for closed-loop system identification. Sel Top Ident Model Control 1996;9:121–8.

[6] Harper D, de Callafon RA, Skelton RE, Talke FE. Piezoelectric stack-based microactuator for hard disk drives. J Inf Storage Process Syst 1999;1:329–32.

[7] Zeng J, de Callafon RA. Model approximation of plant and noise dynamics on the basis of closed-loop data. Proceedings of 13th IFAC symposium on system identification; 2003. pp. 531–6.

[8] Taylor R, Strahle P, Stahl J, Talke F. Measurement of cross-track motion of magnetic tapes. J Inf Storage Process Syst 2000; 2(4).

[9] Ljung L. System identification: theory for the user. 2nd ed. Englewood Cliffs, NJ: Prentice-Hall; 1999.

[10] Zhu YC, Backx T. Identification of multivariable industrial processes for simulation, diagnosis and control. London: Springer; 1993.

[11] Priestley MB. Spectral analysis and time series. London: Academic Press; 1981.